Chiral States in Coupled-Lasers Lattice by On-Site Complex Potential

Sagie Gadasi,* Geva Arwas,* Igor Gershenzon, Asher Friesem, and Nir Davidson
Department of Physics of Complex Systems, Weizmann Institute of Science, Rehovot 7610001, Israel

(Received 30 September 2021; accepted 21 March 2022; published 20 April 2022)

The ability to control the chirality of physical devices is of great scientific and technological importance, from investigations of topologically protected edge states in condensed matter systems to wavefront engineering, isolation, and unidirectional communication. When dealing with large networks of oscillators, the control over the chirality of the bulk states becomes significantly more complicated and requires complex apparatus for generating asymmetric coupling or artificial gauge fields. Here we present a new approach for a precise control over the chirality of the bulk state of a triangular array of hundreds of symmetrically coupled lasers, by introducing a weak non-Hermitian complex potential, requiring only local on-site control of loss and frequency. In the unperturbed network, lasing supermodes with opposite chirality (staggered vortex and staggered antivortex) are equally probable. We show that by tuning the complex potential to an exceptional point, a nearly pure chiral lasing supermode is achieved. While our approach is applicable to any oscillators network, we demonstrate how the inherent nonlinearity of the lasers effectively pulls the network to the exceptional point, making the chirality extremely resilient against noise and imperfections.

DOI: 10.1103/PhysRevLett.128.163901

Introduction.—Chirality is a fundamental property of nature, and the ability to control it is of great scientific and technological importance. In physical systems chiral modes are typically induced by a magnetic field or by its analogs. For example, in the quantum Hall effect, chiral edge currents are generated by magnetic fields [1], in ultracold atoms chiral edge states are induced by artificial gauge fields [2–4], and the rotation direction of hurricanes, depends on the their location on Earth, as a result of Coriolis force. The underlying mechanism in these examples is the breaking of the system's time reversal symmetry, which results in an energy splitting of two, otherwise degenerate, oppositely propagating modes.

In optics, the Faraday effect, induced by a magnetic field, is widely used for breaking time reversal symmetry and inducing directionality [5]. However, the required arrangement is bulky and miniaturizing it to chip-scale size is difficult. Nevertheless, thanks to gain saturation, unidirectional operation of miniature ring lasers can be achieved by asymmetric coupling between the two counterpropagating modes [6–9]. When dealing with a large network of optical oscillators, the control over the supermode's chirality is done by an asymmetric coupling between the individual oscillators. For instance, synthetic magnetic fields allowed the observation of chiral edge states in coupled waveguides [10–13] and the generation of topologically protected chiral edge states in laser arrays [14–16]. While the principle of operation of these methods is intuitive and well studied, asymmetric coupling is usually interferometrically sensitive, requires complicated fabrication facilities, and its implementation in different physical systems is not straightforward.

In this Letter we present an approach for controlling the chirality of a pure bulk state of an arbitrarily large network of nonlinear oscillators, the staggered flux state [17,18], by resorting to a non-Hermitian on-site complex potential [19–22]. Herein, complex potential refers to the combination of frequency detuning and relative loss between the lasers. The complex potential generates an asymmetric energy flow between supermodes with opposite chirality, making one more favorable than the other. Remarkably, the asymmetric energy flow results only from the on-site potential while the coupling between the oscillators remains strictly symmetric, and the "magnetic" flux through each triangular plaquette is exactly zero, in the spirit of the celebrated Haldane model [23,24].

To demonstrate the approach, we consider a triangular lattice of hundreds of symmetrically coupled lasers, in which chiral symmetry is manifested by a two-fold loss-degeneracy of its fundamental lasing supermode. The loss-degeneracy implies that the two supermodes are equally probable upon lasing, and therefore the system's chirality is zero on average. We show that by tuning the complex potential to an exceptional point (EP), it is possible to reach a lasing supermode with a nearly pure chirality. We also show that the lasers' nonlinearity pulls the system towards the EP, making the chiral states extremely robust to noises and disorder.

The presented approach is scalable and can be applied to any number of lasers, to a variety of network geometries, and to other coupled laser systems, such as diode-laser and vertical-cavity-surface-emitting-laser (VCSEL) arrays. Requiring only local on-site control of loss and frequency, the method can be readily applied to force chirality on any

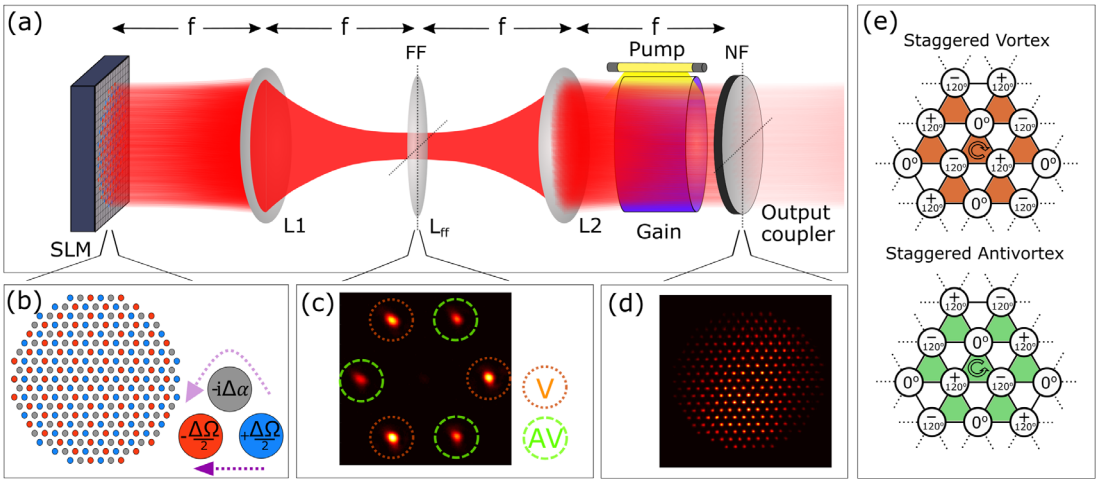

FIG. 1. Experimental arrangement and lasing modes. (a) Schematic arrangement of the digital degenerate cavity laser. (b) The laser network geometry and complex potential that were applied by the SLM. In each triangle, loss of $\Delta\alpha$ was applied to one laser, and a detuning of $\pm(\Delta\Omega/2)$ was applied to the other two lasers. The dashed purple line and curve represent the direct and indirect links between the frequency-detuned lasers. (c) Detected far-field image of the triangular laser lattice without a complex potential ($\Delta\Omega = 0$, $\Delta\alpha = 0$). The spots marked by V (AV) correspond to staggered vortex (antivortex) lasing supermode. The presence of both the V and AV spots is due to the coexistence of multiple uncoupled longitudinal modes, which act as independent realizations of the same experiment. (d) A detected near-field image of the lasers indicating local uniformity of their intensity. (e) Illustration of the two loss-degenerate lasing supermodes of a triangular lattice of negatively coupled lasers, the staggered vortex and staggered antivortex. The circles include the lasers' phases in the different lattice sites, the edges connect nearest neighbors. The orange and green filling colors indicate the triangles' vorticity.

physical systems of coupled oscillators, such as microwave resonators [25], cold atom lattices [26], mechanical systems [27], and even human networks [28].

Experimental arrangement and results.—The approach can be heuristically explained. When two coupled oscillators have a small frequency detuning, they oscillate with a phase difference that is dictated by the detuning [29]. Hence, the frequency detuning induces directionality on the oscillators' phase gradient. For a closed ring of oscillators, one might attempt to achieve chirality by introducing a frequency detuning between two oscillators to enforce a directional phase gradient. However, in a ring, the two oscillators are coupled both directly and indirectly (through the other oscillators in the ring), and for uniform oscillation amplitudes, the detuning actually induces opposite phase gradients on these two links. Therefore the directionality is canceled out and chiral symmetry is maintained [30]. We thus propose to recover the directionality and break the chiral symmetry by weakening the indirect link, by introducing loss to one of the other oscillators [inset of Fig. 1(b)]. We show that an introduction of frequency detuning and loss, a complex potential, indeed induces chirality to an oscillators network (Ref. [36]), and that pure chirality is achieved when the complex potential is tuned to an EP.

To demonstrate control over the chirality of an oscillators network, we use a digital degenerate-cavity laser (DDCL) [37] to set up a triangular lattice of 253 negatively coupled lasers [30]. The DDCL, schematically shown in Fig. 1(a), is comprised of a 4f telescope, an Nd:YAG gain medium, a coupling element, and a spatial light modulator (SLM). The detailed experimental arrangement that includes an 8f telescope is presented in Fig. S1 in the Supplemental Material [30]. The gain medium is pumped by a 200 μs pulsed xenon flash lamp with a 1 Hz repetition rate. The SLM serves as a digital mirror, enabling the generation of laser networks with arbitrary geometry, and accurately controlling the loss and frequency detuning of each of the lasers separately [as in Fig. 1(b)]. The diameter of each laser's mirror is set to 130 μm, and the distance between their centers is set to 300 μm. Negative and symmetric coupling between all nearest-neighbor lasers is achieved by placing a lens with a focal length $f_{\mathrm{FF}} = 5$ m in the far-field (FF) plane, midway between lenses L1 and L2 that form the telescope. This insertion results in light scattered from each laser to its neighbors, so as to couple them. Such an action is mathematically equivalent to the well-known Talbot coupling [38]. An external imaging configuration images the near-field (NF) plane and its Fourier transform, the FF plane. In each laser pulse of the DDCL, many uncoupled longitudinal modes lase simultaneously [39]. Hence, effectively, the detected NF and FF distributions in each lasing pulse are ensemble averages over many independent realizations of the experiment.

Typical FF and NF intensity distributions of the triangular lattice of identical lasers are presented in Figs. 1(c) and 1(d). The two degenerate lasing modes are the staggered vortex (SV) and the staggered antivortex (SAV) modes,

illustrated in Fig. 1(e). The chirality of a lasing mode is encoded in the FF intensity distribution, provided that the lasers intensities are locally uniform [Fig. 1(d)] [30]. The FF of the SV (SAV) mode contains the three spots marked by V (AV) in Fig. 1(c). We quantify the chirality c of the lasing modes by

$$c = \frac{I_{\mathrm{V}} - I_{\mathrm{AV}}}{I_{\mathrm{V}} + I_{\mathrm{AV}}}, \tag{1}$$

where I_{V} and I_{AV} are the average intensities of the V and AV spots.

The loss and frequency detuning of the lasers in the array were modulated according to Fig. 1(b) to form the complex potential. For each triangle in the lattice we added a loss of $\Delta\alpha$ to one of the lasers, and applied a (frequency) detuning of $\pm\frac{1}{2}\Delta\Omega$ to the other two lasers. The detuning $\Delta\Omega$ is the phase that the light accumulates upon reflection from the SLM in every round trip (in radians) [40]. The loss and detuning were applied through the complex reflectivity of the SLM for each laser $R = e^{-\Delta\alpha + i\Delta\Omega}$. The values of the detuning $\Delta\Omega$ and loss $\Delta\alpha$ were varied and the chirality, calculated from the measured FF, is presented in Fig. 2(a). As evident, applying detuning alone ($\Delta\alpha = 0$) or loss alone ($\Delta\Omega = 0$) is not sufficient to induce chirality, in agreement with our heuristic explanation above. We also find that maximal chirality is obtained when the detuning and loss are about equal (marked by the black dashed lines). Three loss cross sections from the two-dimensional diagram are presented in Fig. 2(b). When loss of $\Delta\alpha = 0.15$ is applied, small detuning is already enough to break the system's chiral symmetry. Increasing the detuning results in the increase in chirality up to the point $\Delta\alpha \approx \Delta\Omega$, where nearly pure chirality is obtained. Increasing the detuning further leads to a decrease in the system's chirality. If instead of loss, gain of $\Delta\alpha = -0.15$ is applied, we observe a similar behavior but with the opposite chirality for the same detuning. When no loss is applied ($\Delta\alpha = 0$) and only the detuning is varied, there is no significant change in the system's chirality [41]. Selected FF intensity distributions are presented as insets in Fig. 2(b). The sharp Bragg peaks in the FF measurements indicate on a nearly perfect phase locking of the lasers throughout the array.

Theory and discussion.—To elucidate our experimental results, we begin by analyzing the linear part of the system. As the lasers' evolution is given by the nonlinear laser rate equations (LRE) [30,42], the linear dynamics can be found by setting the gain to zero. To simplify the analysis further, we note that the complex potential breaks the lattice into three sublattices, each by itself has translation symmetry. Hence, by neglecting finite-size corrections, the lattice can be described by an analogous system made of one unit cell of three sites with a modified coupling coefficient $\kappa = 3\tilde{\kappa}$, where $\tilde{\kappa}$ is the coupling strength between two neighboring lasers in the actual lattice. In this linear regime,

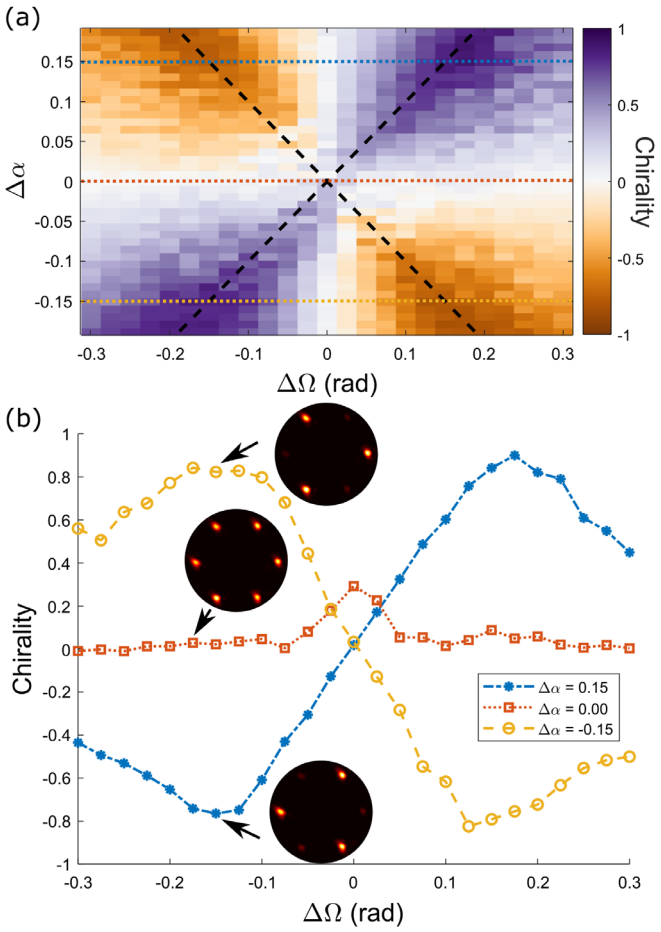

FIG. 2. Experimentally measured chirality, induced by complex potential. (a) The measured chirality c of the lasing mode as a function of the applied frequency detuning $\Delta\Omega$ and relative loss $\Delta\alpha$. Maximal chirality is obtained along the lines $\Delta\Omega = \Delta\alpha$, marked by the black dashed lines. (b) Cross sections of the chirality for varying $\Delta\Omega$ at fixed $\Delta\alpha$ values [marked by the dotted colored lines in (a)]. The measurement points are connected by lines. Insets show typical far-field images at selected points.

the evolution of the electric field in the cavities of one unit cell is governed by a Schrödinger-like equation, $(d\boldsymbol{E}/dt) = -i\mathcal{H}\boldsymbol{E}$, where

$$\mathcal{H} = \begin{pmatrix} -\frac{1}{2}\Delta\Omega & -i\kappa & -i\kappa \\ -i\kappa & -i\Delta\alpha & -i\kappa \\ -i\kappa & -i\kappa & +\frac{1}{2}\Delta\Omega \end{pmatrix} \tag{2}$$

is the Bloch Hamiltonian, and $\boldsymbol{E}$ is a column vector of the electric field on the three sites [30]. The imaginary coupling coefficients correspond to a dissipative (non energy-conserving) coupling [43,44]. Without $\Delta\Omega$ and $\Delta\alpha$, the system's eigenmodes are the vortex, antivortex, and uniform phase mode. The introduction of $\Delta\Omega$ or $\Delta\alpha$ breaks the system's invariance for rotation in $(2\pi/3)$, and therefore the vortex and antivortex modes are no longer eigenmodes of

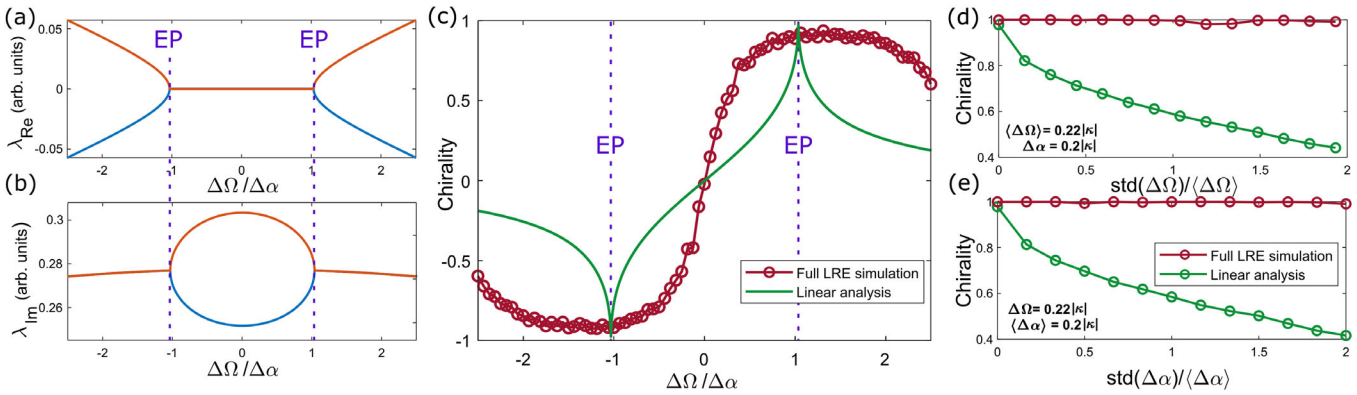

FIG. 3. Theoretical analysis. (a) and (b) The real and imaginary parts of the eigenvalues of the linear system's minimal loss eigenmodes as a function of $\Delta\Omega$ and fixed $\Delta\alpha$. Exceptional points, marked by the vertical purple dashed lines, emerge at $\Delta\Omega_{EP} \approx 1.1\Delta\alpha$ (for $\Delta\alpha = 0.08\kappa$), where a square-root splitting is apparent. The blue and orange curves correspond to the two eigenvalues of $\mathcal{H}$ with the lowest imaginary part. (c) Chirality of a three-laser system. The solid green curve presents the chirality of the minimal-loss eigenmode of the linear system. The red circles display the chirality of the laser network, obtained from simulation of the nonlinear laser rate equations. (d) and (e) The calculated averaged chirality of a triangular lattice with a noisy complex potential. The chirality of the minimal-loss cold-cavity linear mode (green circles) and the chirality of the nonlinear laser network (red circles) are displayed as a function of the standard deviation of the normal distribution from which the complex potential is drawn. In (d) $\Delta\alpha$ is held constant while in (e) $\Delta\Omega$ is constant. The mean values are displayed, and correspond to an exceptional point. The data points in (c)–(e) are connected by a solid line.

the system. The loss and frequency associated with each of the system's new eigenmodes are given by the imaginary and real parts of the corresponding eigenvalues $\{\lambda\}$, and are presented in Figs. 3(a) and 3(b) for fixed $\Delta\alpha$, and varying $\Delta\Omega$. The transition of the eigenvalues from having a degenerate imaginary part to having a degenerate real part is attributed to the breaking of anti-parity-time symmetry [30,45]. An EP [46], a non-Hermitian degeneracy at which the two eigenmodes become identical, emerges when the detuning is adjusted to specific values: $\Delta\Omega_{EP} \approx \pm\Delta\alpha$ [30]. At the EP, the two eigenmodes collapse into a nearly pure vortex or antivortex mode [30]. The eigenmodes chirality, calculated from their projection on the vortex and antivortex modes and according to Eq. (1), is displayed in Fig. 3(c) by the solid green line. When $\Delta\alpha$ is applied, and $\Delta\Omega$ is raised from zero, chirality emerges and increases up to the EP, where the eigenmodes become a pure vortex or a pure antivortex. Increasing $\Delta\Omega$ further results in a decrease in the chirality.

Juxtaposing the linear-analysis results and the experimental results reveals a very good correspondence. The linear-analysis explains the emergence of chirality, and its behavior as a function of the applied complex potential. Also, evidence of the EPs at $\Delta\Omega_{EP} \approx \pm\Delta\alpha$, where the eigenmodes have nearly pure chirality are present in Fig. 2(a) at the predicted locations. Nevertheless, the experimental chirality peaks in Fig. 2(b) are significantly broadened relative to the linear analysis [Fig. 3(c)]. This is also manifested in the broad chiral lines along $\Delta\Omega = \pm\Delta\alpha$ in Fig. 2(a), where small changes in the detuning or loss have a small effect on the chirality of the lasing mode. We show below that this striking difference emerges from the system's nonlinearity.

A more complete description of the system is obtained by numerically solving the full nonlinear LRE. Simulations results reveal that the lasing mode at steady state is either a vortex or an antivortex mode, rather than a superposition of the two, and that the outcome of varying the value of $\Delta\Omega$ for a fixed $\Delta\alpha$ is a change in the probability to get one mode over the other [30]. The red curve in Fig. 3(c) shows the chirality obtained from numerical simulations of the LRE of three lasers on a triangle with the experimental parameters, averaged over 1000 realizations (each starts with a different random electric field distribution) [30]. The simulations reproduce the broad pure-chirality peaks around the EPs, in agreement with the experimental results.

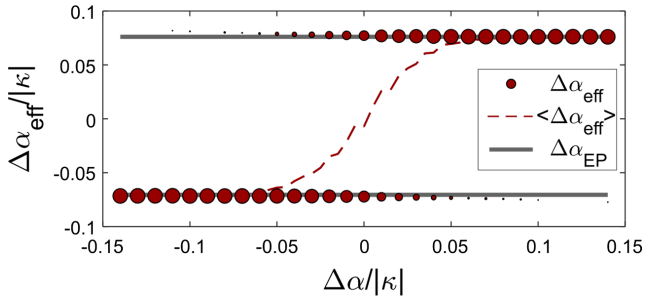

FIG. 4. Simulation results for the effective loss $\Delta\alpha_{eff}$ (red circles) as a function of the applied loss $\Delta\alpha$ for a fixed $\Delta\Omega = 0.085|\kappa|$ and unsaturated gain of $g_0 = 1.2g_{0,th}$, where $g_{0,th}$ is the unsaturated gain at the lasing threshold. The circles' diameter represents the prevalence of $\Delta\alpha_{eff}$ among the 1000 realizations. The dashed line shows an ensemble average $\langle\Delta\alpha_{eff}\rangle$. It is evident that $\Delta\alpha_{eff}$ approaches the values of $\Delta\alpha_{EP}$ (horizontal lines). The lasers' nonlinearity pulls the system to the EPs. Similar results obtained for other values of $\Delta\Omega$ and g_0 [30].

To further investigate the chiralilty's robustness to imperfections of the complex potential, we performed simulations of a triangular lattice comprised of 72 lasers with periodic boundary conditions and noisy complex potential. In the simulations, the mean value of the complex potential was set to an EP, and either $\Delta\Omega$ [Fig. 3(d)] or $\Delta\alpha$ [Fig. 3(e)] of each of the lasers was randomly drawn from a normal distribution with a varying standard deviation. The mode's chirality was calculated similarly to Fig. 3(c) for both the linear and nonlinear regimes. As is evident, the chiral modes in the nonlinear system are significantly more robust to noises in the complex potential.

The chirality's resilience to deviations of the complex potential from its value at the EP is a consequence of the lasers' nonlinearity. In the steady state, the effective loss between the lasers is given by $\Delta\alpha_{\mathrm{eff}} = \Delta\alpha - \Delta G$, where ΔG is the difference in the nonlinear gain between the lossy laser and the other lasers in the triangle [30]. Simulation results reveal that nonlinearity modifies $\Delta\alpha_{\mathrm{eff}}$ exactly to bring the system to an EP, for the applied detuning ($\Delta\alpha_{\mathrm{EP}}$), as demonstrated in Fig. 4. The nonlinearity thus provides extreme robustness of the chirality against noises and perturbations, making this approach appealing for practical applications and large scale fabrication.

Conclusions.—In this work we showed experimentally that the introduction of an on-site complex potential to a triangular lattice of hundreds of symmetrically coupled lasers, drives the system to a well-controlled pure chiral supermode of staggered vortex or staggered antivortex. We also showed that the chirality is maximized when the complex potential is tuned to the EPs of the linear system. At the EPs the eigenmodes of the linear system merge into pure chiral states. Moreover, the gain nonlinearity directs the effective relative loss between the lasers towards its value at the EP, making the system's chirality remarkably resilient to loss and detuning noises. The presented approach is scalable and can be applied to any number of lasers, to various network geometries, and to other physical systems. It may lead to new insights in synchronization, topology of complex band structures [47,48], novel non-Hermitian symmetries, and spin simulators [49].

The authors thank Oren Raz and Nitsan Bar for fruitful discussions.

S. G. and G. A. contributed equally to this work.

[*] These authors contributed equally to this work.
[1] R. B. Laughlin, Phys. Rev. B **23**, 5632 (1981).
[2] M. Mancini, G. Pagano, G. Cappellini, L. Livi, M. Rider, J. Catani, C. Sias, P. Zoller, M. Inguscio, M. Dalmonte, and L. Fallani, Science **349**, 1510 (2015).
[3] Y.-J. Lin, R. L. Compton, K. Jiménez-García, J. V. Porto, and I. B. Spielman, Nature (London) **462**, 628 (2009).
[4] J. Dalibard, F. Gerbier, G. Juzeliunas, and P. Öhberg, Rev. Mod. Phys. **83**, 1523 (2011).
[5] L. J. Aplet and J. W. Carson, Appl. Opt. **3**, 544 (1964).
[6] J. P. Hohimer, G. A. Vawter, and D. C. Craft, Appl. Phys. Lett. **62**, 1185 (1993).
[7] B. Peng, Ş. K. Özdemir, M. Liertzer, W. Chen, J. Kramer, H. Yılmaz, J. Wiersig, S. Rotter, and L. Yang, Proc. Natl. Acad. Sci. U.S.A. **113**, 6845 (2016).
[8] P. Miao, Z. Zhang, J. Sun, W. Walasik, S. Longhi, N. M. Litchinitser, and L. Feng, Science **353**, 464 (2016).
[9] Z. Zhang, X. Qiao, B. Midya, K. Liu, J. Sun, T. Wu, W. Liu, R. Agarwal, J. M. Jornet, S. Longhi, N. M. Litchinitser, and L. Feng, Science **368**, 760 (2020).
[10] M. Hafezi, S. Mittal, J. Fan, A. Migdall, and J. M. Taylor, Nat. Photonics **7**, 1001 (2013).
[11] M. C. Rechtsman, J. M. Zeuner, Y. Plotnik, Y. Lumer, D. Podolsky, F. Dreisow, S. Nolte, M. Segev, and A. Szameit, Nature (London) **496**, 196 (2013).
[12] K. Fang, Z. Yu, and S. Fan, Nat. Photonics **6**, 782 (2012).
[13] L. Lu, J. D. Joannopoulos, and M. Soljačić, Nat. Photonics **8**, 821 (2014).
[14] M. A. Bandres, S. Wittek, G. Harari, M. Parto, J. Ren, M. Segev, D. N. Christodoulides, and M. Khajavikhan, Science **359**, eaar4005 (2018).
[15] H. Zhao, X. Qiao, T. Wu, B. Midya, S. Longhi, and L. Feng, Science **365**, 1163 (2019).
[16] Z. Yang, E. Lustig, G. Harari, Y. Plotnik, Y. Lumer, M. A. Bandres, and M. Segev, Phys. Rev. X **10**, 011059 (2020).
[17] J. Struck, M. Weinberg, C. Ölschläger, P. Windpassinger, J. Simonet, K. Sengstock, R. Höppner, P. Hauke, A. Eckardt, M. Lewenstein, and L. Mathey, Nat. Phys. **9**, 738 (2013).
[18] M. Aidelsburger, M. Atala, S. Nascimbène, S. Trotzky, Y.-A. Chen, and I. Bloch, Phys. Rev. Lett. **107**, 255301 (2011).
[19] A. Ghatak and T. Das, J. Phys. Condens. Matter **31**, 263001 (2019).
[20] Q.-B. Zeng, B. Zhu, S. Chen, L. You, and R. Lü, Phys. Rev. A **94**, 022119 (2016).
[21] S. Longhi, Phys. Rev. A **93**, 022102 (2016).
[22] L. E. F. F. Torres, J. Phys. **3**, 014002 (2019).
[23] F. D. M. Haldane, Phys. Rev. Lett. **61**, 2015 (1988).
[24] G. Jotzu, M. Messer, R. Desbuquois, M. Lebrat, T. Uehlinger, D. Greif, and T. Esslinger, Nature (London) **515**, 237 (2014).
[25] K. M. Sliwa, M. Hatridge, A. Narla, S. Shankar, L. Frunzio, R. J. Schoelkopf, and M. H. Devoret, Phys. Rev. X **5**, 041020 (2015).
[26] C. Gross and I. Bloch, Science **357**, 995 (2017).
[27] R. Süsstrunk and S. D. Huber, Science **349**, 47 (2015).
[28] S. Shahal, A. Wurzberg, I. Sibony, H. Duadi, E. Shniderman, D. Weymouth, N. Davidson, and M. Fridman, Nat. Commun. **11**, 3854 (2020).
[29] J. A. Acebrón, L. L. Bonilla, C. J. Pérez Vicente, F. Ritort, and R. Spigler, Rev. Mod. Phys. **77**, 137 (2005).
[30] See Supplemental Material at http://link.aps.org/supplemental/10.1103/PhysRevLett.128.163901 for detailed experimental arrangement, equations derivation, and additional numerical simulation results. The Supplemental Material includes Refs. [31–35].
[31] S. Ngcobo, I. Litvin, L. Burger, and A. Forbes, Nat. Commun. **4**, 2289 (2013).
[32] V. Evtuhov and A. E. Siegman, Appl. Opt. **4**, 142 (1965).
[33] J. A. Arnaud, Appl. Opt. **8**, 189 (1969).

[34] I. Gershenzon, G. Arwas, S. Gadasi, C. Tradonsky, A. Friesem, O. Raz, and N. Davidson, Nanophotonics **9**, 4117 (2020).
[35] C. Tradonsky, V. Pal, R. Chriki, N. Davidson, and A. A. Friesem, Appl. Opt. **56**, A126 (2017).
[36] For coupled lasers, applying only frequency detuning may lead to the emergence of chiral modes in some cases. However, the mechanism remains similar: The oscillation amplitude of one laser is reduced (due to nonlinearity) and thus weakens the indirect link [30].
[37] C. Tradonsky, I. Gershenzon, V. Pal, R. Chriki, A. A. Friesem, O. Raz, and N. Davidson, Sci. Adv. **5**, eaax4530 (2019).
[38] S. Mahler, C. Tradonsky, R. Chriki, A. A. Friesem, and N. Davidson, OSA Continuum **2**, 2077 (2019).
[39] S. Mahler, M. L. Goh, C. Tradonsky, A. A. Friesem, and N. Davidson, Phys. Rev. Lett. **124**, 133901 (2020).
[40] The frequency detuning $\Delta\Omega$ can be translated to units of frequency by multiplying $\Delta\Omega$ by $(\mathrm{FSR}/2\pi)$, where $\mathrm{FSR} = 60$ MHz is the free spectral range of the lasers.
[41] The relatively weak chirality measured at $\Delta\alpha = 0$ and $\Delta\Omega = 0$ is attributed to imperfections in the cavity alignment, which break the degeneracy between the V and AV modes.
[42] F. Rogister, K. S. Thornburg, L. Fabiny, M. Möller, and R. Roy, Phys. Rev. Lett. **92**, 093905 (2004).
[43] Because of the dissipative nature of the Hamiltonian, steady state solutions other than $\boldsymbol{E} = 0$ can be obtained only if sufficient gain is introduced, but for the linear analysis at this step, only the eigenmodes of Eq. (2) are of interest.
[44] J. Ding, I. Belykh, A. Marandi, and M.-A. Miri, Phys. Rev. Applied **12**, 054039 (2019).
[45] P. Peng, W. Cao, C. Shen, W. Qu, J. Wen, L. Jiang, and Y. Xiao, Nat. Phys. **12**, 1139 (2016).
[46] M.-A. Miri and A. Alù, Science **363**, eaar7709 (2019).
[47] K. Kawabata, K. Shiozaki, M. Ueda, and M. Sato, Phys. Rev. X **9**, 041015 (2019).
[48] M. G. Reuter, J. Phys. Condens. Matter **29**, 053001 (2017).
[49] P. L. McMahon, A. Marandi, Y. Haribara, R. Hamerly, C. Langrock, S. Tamate, T. Inagaki, H. Takesue, S. Utsunomiya, K. Aihara, R. L. Byer, M. M. Fejer, H. Mabuchi, and Y. Yamamoto, Science **354**, 614 (2016).